What Can we Learn from Nonequilibrium Response of a Strange Metal?[1]

B. A. Polyak[+][*], V. S. Khrapai[*], E. S. Tikhonov[*] [2]

[+]*Moscow Institute of Physics and Technology, 141700 Dolgoprudny, Russia*

[*]*Osipyan Institute of Solid State Physics of the Russian Academy of Sciences, 142432 Chernogolovka, Russia*

We critically address the recent experiment by L. Chen et al. [Science **382**, 907 (2023)] on nonequilibrium transport and noise in a strange metal $YbRh_2Si_2$ patterned into the nanowire shape. In the long device, resistivity, differential resistance and current noise data seem to be consistent allowing us to extract electron-phonon coupling and the temperature dependence of electron-phonon scattering length. The obtained values can be reconciled with the experimental data for the short device only assuming the significant contact resistance. We discuss its possible origin as due to the current redistribution between $YbRh_2Si_2$ and its gold covering, and reveal that this redistribution contact resistance should be proportional to the $YbRh_2Si_2$ resistivity. We also discuss some subtleties of the noise measurements. Overall, neglecting electron-phonon energy relaxation even in the shortest devices is arguable so that the observed shot noise suppression can hardly be attributed to the failure of quasiparticle concept.

I. Introduction. The origin of strange metal behavior which is manifested in the linear temperature (T) dependence of resistivity down to lowest T in some materials [1–5], remains without generally accepted theoretical explanation [6–12]. On the experimental side, beyond common resistivity measurements novel approaches [13–15] are required. In particular, the recent paper by Liyang Chen et al. [15] reports on the measurements of shot noise in the heavy fermion strange metal $YbRh_2Si_2$ patterned into the nanowire shape. The authors claim that the observed shot noise suppression can not be attributed to the electron-phonon energy relaxation in a standard Fermi liquid model but rather indicates the failure of quasiparticle concept. This interpretation has been criticized [16, 17] which motivated us to consider in the present manuscript the peculiarities of the nonequilibrium transport approach to the study of strange metals. In our letter we show that electron-phonon scattering is most likely strong enough to suppress shot noise even in the presented short devices which makes the statement on the failure of quasiparticle concept [15] arguable. At the same time, resistance and noise data from the long device can be con-

sistently explained and thus provide important information about electron-phonon coupling which is essential for further transport experiments.

Figure 1a demonstrates the sketch of studied devices. Patterned from a $t = 60\,$nm thick $YbRh_2Si_2$ film (gray) with resistivity ρ, grown on germanium substrate, they are represented by nanowire-shaped constrictions of length L and width w, connected to source and drain pads. As shown by yellow shading, these two pads are additionally covered with 200 nm of gold. We note that at low bath temperature (T_0) the gold conductivity is approximately 10 times higher than that of $YbRh_2Si_2$ (at 3 K). Bottom part of Fig. 1a shows schematically the current density vector both in $YbRh_2Si_2$ and in gold covering in the region where current redistributes between the two layers. This region extends for the so-called current transfer length λ depending on the quality of the $YbRh_2Si_2$/Au interface which we quantify with the interface conductance per unit area, σ_{int}. Overall, the authors provide data for three devices with short constrictions, $L \lesssim 1\,\mu$m, further refered to as short devices, and for one device with long constriction, $L = 28\,\mu$m, further referred to as long device. The widths of all nanowires range from 140 to 300 nm. We estimate geometric dimensions of all constrictions from the available scanning electron micrograph images. As we argue in this manuscript, geometry of the devices may require taking into account

---

the contribution to the measured resistance and noise not only from the nanowires themselves but also from the significant part of the pads.
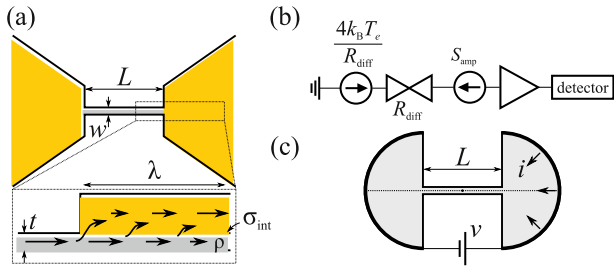

Fig. 1. (Color online) Device geometry and measurement setup. (a) – Schematic representation of a device. YbRh$_2$Si$_2$ film $t = 60$ nm thick (gray) is patterned into a constriction connecting two pads. These pads are additionally covered with 200 nm of gold (yellow). The length and the width of the constriction are L and w, respectively. Interface between YbRh$_2$Si$_2$ and gold is characterized by conductivity $\sigma_{\rm int}$, current transfer length is λ. (b) – Equivalent circuit of noise measurement setup. (c) – Geometry used in numerical modelling. We calculate the total current through the constriction, i, in response to the applied bias voltage, v

II. Long device.

A. Differential resistance. We start our discussion with the analysis of experimental data for the long device. Here, the central constriction is approximately 30 times longer than that for three short devices so that the possible effect of the interface may be most likely neglected. Below we show that electron-phonon scattering length in YbRh$_2$Si$_2$ is $l_{e-ph}(3\,{\rm K}) \approx 1\,\mu$m and decreases with increasing temperature. This ensures that in the presence of bias current I electron system in the long constriction is described by position-independent electronic temperature $T_e(I)$ everywhere besides short regions near the pads. At all T_0 this dependence can be obtained using a standard procedure. From the differential resistance data provided in Supplementary Materials Fig. S3B [15], we extract $R = V/I$ at $T_0 = 3, 5$ and 7 K. Further, attributing the growth of $R(I)$ with increasing current to the increase of T_e, we extract $T_e(I)$. Here, we use the fact that the T-dependence of the normalized resistance of the devices is demonstrated to be the same as that for the unpatterned film, see Fig. 1C [15]. The obtained curves $T_e(I)$ are shown in Fig. 2a. Without noise measurements, these data already allow one to estimate electron-phonon coupling which describes the power flow from electron to phonon subsystem via

$$P_{e-ph} = \mathcal{V}\Sigma_{e-ph}(T_e^n - T_{ph}^n),$$

where $\mathcal{V}$ is the system volume, T_{ph} is the phononic temperature and the exponent n typically varies in the range $n \approx 3-5$ [18]. The devices are patterned on crystalline germanium substrates ensuring $T_{ph} = T_0$. In a steady state $P_{e-ph} = P_J$, where P_J is the released Joule heat power so that

$$P_J = \mathcal{V}\Sigma_{e-ph}(T_e^n - T_0^n). \tag{1}$$

In Figure 2b we show that $n = 4.7$ fits the data perfectly with $\Sigma_{e-ph} = 9.6 \cdot 10^8$ W/K$^{4.7}$m^3 (we take $w = 300$ nm). From here, we extract the T-dependence of the electron-phonon scattering length using [19]

$$l_{e-ph} = L\left[\mathcal{L}/nT^{n-2}\mathcal{V}\Sigma_{e-ph}R(T)\right]^{1/2},$$

where $\mathcal{L} = 2.44 \cdot 10^{-8}$ WΩK^{-2} is the Lorenz number. The result is shown in Fig. 2c and in the given temperature range can be reasonably approximated as $l_{e-ph} \propto \propto T^{-1.7}$, see the dashed line. Importantly, $l_{e-ph}(3\,{\rm K}) \approx \approx 1.4\,\mu$m ensuring the possibility to introduce position-independent electronic temperature $T_e(I)$ which will be further used in noise treatment.

B. Nonequilibrium noise. Before discussing nonequilibrium noise of the long device, we note some general details of the noise measurements. In the setup used in [15], see Fig. 1b for the schematic circuit, the voltage noise before amplification is determined by two contributions,

$$S_V(I) = \left[\frac{4k_{\rm B}T_e(I)}{R_{\rm diff}(I)} + S_{\rm amp}\right]R_{\rm diff}^2(I), \tag{2}$$

where $R_{\rm diff} = dV/dI$ is the differential resistance of the device, T_e is its average electronic temperature, the first term comes from the current noise of the device itself, the second term is defined by the parasitic input current noise of the amplifiers, $S_{\rm amp}$, and $S_V(0)$ is the voltage noise in equilibrium. Note that in the nonlinear regime $R_{\rm diff}$ depends on I so that $S_{\rm amp}$ contributes to the measured excess voltage noise. Whether one can neglect $S_{\rm amp}$ or not, depends on the interplay between the two terms in (2). Therefore, along with determining the gain it is also the goal of calibration to get the magnitude of amplifier noise. Typically, when one uses homemade voltage amplifier at liquid helium temperature, its input current noise is on the order of 10^{-27} A^2/Hz [20–22] where the precise value depends on the used transistor, operating frequency and device resistance [23]. The authors of [15] use room-temperature commercial preamplifiers, low-noise LI-75 and SR-560 which is usually not used in noise measurements. One can therefore expect $S_{\rm amp} \gtrsim 10^{-25}$ A^2/Hz. We note that this current noise can not be extracted from the setup
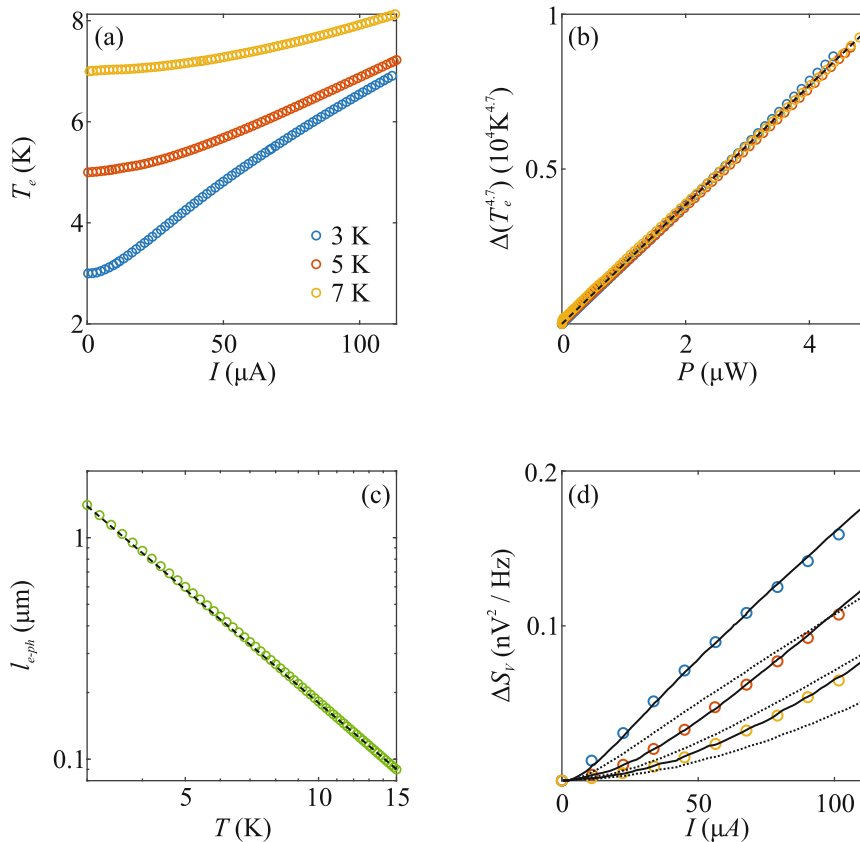
Fig. 2. (Color online) Nonequilibrium response of the long nanowire. (a) – Electronic temperature of the nanowire as a function of bias current. (b) – Electron-phonon power flow obeys $P = \mathcal{V}\Sigma_{e-ph}(T_e^{4.7} - T_{ph}^{4.7})$ with $\Sigma_{e-ph} = 9.6 \cdot 10^8$ W/K$^{4.7}$m^3. (c) – Electron-phonon scattering length as a function of temperature. Dashed line is $l_{e-ph} \propto T^{-1.7}$. (d) – Excess voltage noise spectral density of the device, $\Delta S_V = S_V(I) - S_V(0)$, as a function of bias current. Symbols represent the data from the experiment [15]. Both dotted and solid lines correspond to $\Sigma_{e-ph} = 9.6 \cdot 10^8$ W/K$^{4.7}$m^3 but with $S_{\mathrm{amp}} = 0$ and $S_{\mathrm{amp}} = 5 \cdot 10^{-25}$ A^2/Hz, respectively

calibration discussed in Supplementary Material Section 2 [15]. Namely, the calibration was performed by detecting the room temperature thermal noise of a variety of resistors, see Supplementary Material Fig. S1. At room temperature, the current noise of a typical used $100\,\Omega$ resistor is $1.6 \cdot 10^{-22}$ A^2/Hz and by far exceeds the expected value of S_{amp} so that the presented calibration procedure is absolutely helpless in its determination. At the same time, the current noise of a strange metal long device cooled down to $5\,\mathrm{K}$ and with a resistance of approximately $300\,\Omega$ is $9 \cdot 10^{-25}$ A^2/Hz which may easily be comparable to the expected value of S_{amp}. In other words, the setup calibration is performed for the values of current noise which are two orders of magnitude greater than those utilized in the experiment.

The value of S_{amp} in the experiment can be estimated by comparison of experimental results for the voltage fluctuations of the long device, see Supplementary Material Fig. S3A of [15], to what one can expect based on the obtained curves $T_e(I)$ presented in Fig. 2a. By solid lines in Fig. 2d we show the best fits to the experimental data (symbols) of [15]. These fits are obtained using (2) with $S_{\mathrm{amp}} = 5 \cdot 10^{-25}$ A^2/Hz which perfectly falls in the above order of magnitude expectation. We emphasize that considering current noise of the device in the form of thermal noise with electronic temperature elevated above bath temperature in (2) is valid in the presence of strong electron-phonon scattering. Dotted lines additionally illustrate the fits obtained with zero preamplifier noise. Note these fits go below the experimental data indicating contribution of the parasitic noise.

As a final remark, we note that the obtained above T-independent value of Σ_{e-ph} implies the temperature dependence of $\Gamma = (e/k_{\mathrm{B}})^2 \Sigma_{e-ph}/\sigma$ since conductivity changes by approximately 40% in the temperature range from 3 to 7 K. At the same time, the authors of [15] used in their fits T-independent $\Gamma \approx 9 \cdot 10^9$ K^{-3}m^{-2}, see Sec-

tion 5 in Supplementary Material. This difference may explain the better quality of our fits for the differential resistance.

III. Short devices.

A. Contact resistance. We now discuss the short device ($L = 660\,\text{nm}$) presented in the main text, see Fig. 2A [15]. Given the width of the constriction is close to that of the long nanowire, one might have expected its linear response resistance at $3\,\text{K}$ to be around $6\,\Omega$. The actual value is $36\,\Omega$ demonstrating there is significant inconsistency between formally extracted resistivities of the two devices. Note that additional data on two more short devices presented in Supplementary Material Fig. S5 reveal the similar discrepancy. In principle, this inconsistency can partly be attributed to the nanoscale patterning of the devices using reactive ion etching which inevitably damages the edges of the constrictions (L. Chen and D. Natelson, private communication). Figure 1(C, D) of [15] compares temperature and magnetic field (B) behavior of the unpatterned film with that of the nanowire-patterned device and demonstrates similar results in terms of normalized resistances. Therefore, while there is approximately 6-fold difference in the resistivities we believe that the underlying physics is still there so that damaged edges are hardly responsible for the discussed inconsistency. The authors of [15] use Fig. 1(C, D) to claim that the total resistance of the device is dominated by the constrictions and the pads contribution is negligible. Below we explain that this argument is in fact incorrect and the pads contribution, which we further refer to as contact resistance, can not be excluded based on the observation of similar for the film and for the patterned devices $R(T)$ and $R(B)$ dependences.

To illustrate the idea, we consider the geometry depicted in the bottom part of Fig. 1a. Further, we take gold conductivity to be infinitely large. Upon leaving the constriction, current starts to redistribute between the YbRh$_2$Si$_2$ film and the gold cover. This redistribution stops after going distance λ deep inside the pad along the interface. This distance is called the current transfer length and depends on the film resistivity and on the interface conductivity, σ_{int}. For $\sigma_{\text{int}} = 0$ current doesn't flow over the interface and remains completely in the YbRh$_2$Si$_2$ film. In this case, the contact resistance is log-divergent with the contact size a as $R_1(a) = \rho \ln(2a/w)/(\pi t)$. On the other hand, if all voltage drop occurs across the interface between the two layers, which happens for $\rho = 0$, the contact resistance is $R_2(a) = 2/(\pi a^2 \sigma_{\text{int}})$. In an infinite contact with both ρ and σ_{int} finite, the reasonable quantitative estimate for both the current transfer length and the contact resis-

tance is obtained from $R_1(\lambda) = R_2(\lambda) \sim R_{\text{cont}}$, that is

$$\frac{\rho}{\pi t} \ln\left(\frac{2\lambda}{w}\right) = \frac{2}{\pi \lambda^2 \sigma_{\text{int}}} \sim R_{\text{cont}}.$$

In Supplemental Material we provide the analytical solution and demonstrate that in the limit of large enough $\lambda \gg w$ the above estimate reproduces the exact result up to only a $10\,\%$ correction for the logarithm argument. Importantly, the T-dependence of λ is weak and closely follows $\lambda \propto \rho^{-1/2}$. Therefore, up to an unimportant log-factor the contact resistance is proportional to the YbRh$_2$Si$_2$ resistivity,

$$R_{\text{cont}} \propto \rho. \tag{3}$$

As a result, observation of the identical T and B response for the parent film and for the patterned device doesn't ensure negligible contact resistance. We also note that for the realistic finite-size devices contact resistance may further be enlarged due to the factors not considered in this idealized picture. In Supplemental Material we show that the T-dependence of linear-response resistance for the short device presented in the main text, see Fig. 2A [15], is reasonably approximated using $\lambda(3\,\text{K}) \approx 280\,\mu\text{m}$ which is comparable to the pads size and indicates the possible importance of current redistribution effect.

B. Differential resistance. Given the great difference between the expected and the observed resistance of short devices, we argue that the current transfer length may exceed the dimensions of constrictions by orders of magnitude and be comparable to or even exceed the dimensions of devices with pads included. To numerically simulate the differential resistance, we choose the geometry of Fig. 1c. Here, the radius of pads equals $20\,\mu\text{m}$ and the current redistribution on the lateral scale of these pads is neglected. The electrodes are indicated by thick black lines. On the one hand, this geometry is close to the geometry of the patterned film nearby the constriction in real devices. On the other hand, the scale of $20\,\mu\text{m}$ is large enough to capture the nonlinearity of differential resistance, since due to $l_{e-ph} \lesssim 1\,\mu\text{m}$ electronic temperature in the presence of current reaches the value of T_0 on the spatial scale of few micrometers beyond the constriction. Additionally, crucial to the numerical calculations for this highly nonuniform geometry, thus chosen size is not too large to require inadequate computing power.

We first implement our numerical approach for the long device. Symbols in the top panel of Fig. 3a reproduce the experimental data from the Supplementary Material Fig. S3B [15]. Solid lines are fits obtained with $\Sigma_{e-ph} = 6.1 \cdot 10^8\,\text{W/K}^5\text{m}^3$ and $n = 5$ in (1)
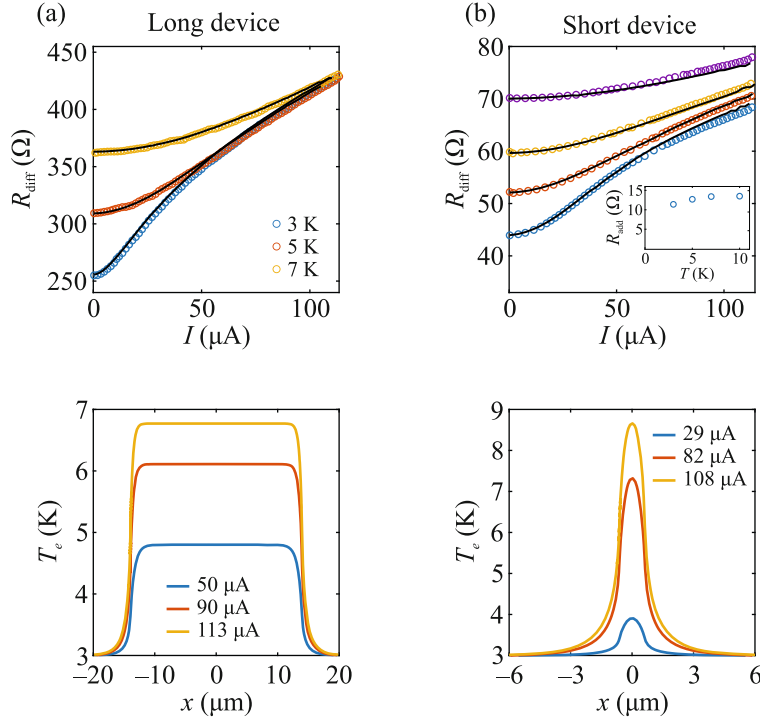
Fig. 3. (Color online) Numerical simulation of nonequilibrium response for both: (a) – long and (b) – short (device #3) constrictions. Symbols in top panels reproduce the experimental results of [15] for differential resistance as a function of bias current. Solid lines are fits obtained with numerical simulation (see text). The inset of top panel in (b) demonstrates the T-dependence of the bias-independent contact resistance. The bottom panels demonstrate the spatial profile of electronic temperature along the dashed line depicted in Fig. 1c with $x = 0$ corresponding to the center of the constriction

and the T-dependence of YbRh$_2$Si$_2$ resistivity $\rho(T) = 10.8 + 1.67\,T\,[\mu\Omega \cdot \text{cm}]$ which captures the linear-response resistance data and fits the data of Fig. 1C [15] with better than 10 % accuracy in the temperature range below 10 K. Note that the difference between thus obtained Σ_{e-ph} and the value extracted from Fig. 2b is due to the slightly different power-law of electron-phonon cooling rate. The spatial profile of electronic temperature along the dashed line depicted in Fig. 1c is demonstrated in the bottom panel of Fig. 3a with $x = 0$ corresponding to the center of the constriction.

Having extracted Σ_{e-ph}, we attempt to fit the bias dependence of differential resistance for one of short devices. For this purpose we choose the device #3 from Supplementary Material Fig. S5E [15]. Among the overall presented three short devices, this is the narrowest one so that we expect the contact resistance to be significant enough but not dominating over the constriction resistance compared with two other short devices. Note also that while the constriction of this device is approximately two times narrower than the constriction of the device #2 from Supplementary Material Fig. S5(A-C), its resistance is only $\approx 30\,\%$ greater which again may indicate the significant contact resistance in all short

devices. We take the length and the width of the constriction in device #3 to be $l = 1.3\,\mu$m and $w = 155$ nm, respectively; the corresponding resistivity is taken to be the same as for the long device. Symbols in the top panel of Fig. 3b reproduce the experimental data from the Supplementary Material Fig. S5E [15]. Solid lines are fits obtained with

$$R_{\text{diff}} = \frac{dv}{di} + R_{\text{add}}(T),$$

where v is the voltage applied between two electrodes in Fig. 1c, i is the calculated current and $R_{\text{add}}(T)$ is chosen as current-independent quantity to fit the linear-response resistance for all four temperatures of interest. R_{add} must include, at least, the contribution to contact resistance due to current redistribution across the imperfect YbRh$_2$Si$_2$/gold interface beyond the semicircular pads depicted in Fig. 1c. Additional contribution to R_{add} may come from finite gold resistivity and possibly present interface defects. Taking into account only current redistribution effect, in accordance with (3) one should expect $R_{\text{add}} \propto \rho$. In the inset we demonstrate the obtained $R_{\text{add}}(T)$ dependence which turns out to be slower than $\rho(T)$ indicating that current redistribution
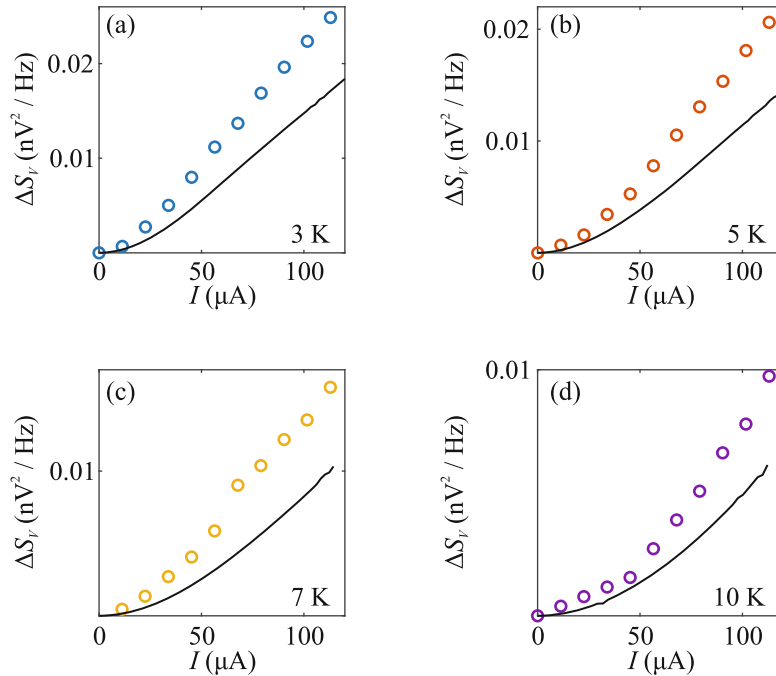
Fig. 4. (Color online) Numerical simulation of nonequilibrium noise for the device #3. Symbols represent the data from the experiment [15] for excess voltage noise as a function of bias current. Solid lines are fits calculated using the position-dependent electronic temperature similar to the bottom panel of Fig. 3b (see text)

is not the only effect contributing to the contact resistance. Additionally, in the bottom panel of Fig. 3b we plot the spatial profile of electronic temperature along the short constriction. Both bottom panels of Fig. 3 verify that electron-phonon scattering is strong enough so that the devices can not be considered as in phase-coherent regime which was recently analyzed theoretically [24].

C. Nonequilibrium noise. Finally, we compare the experimental results for nonequilibrium noise in the short device with what we expect based on the spatial temperature profile demonstrated in Fig. 3d. By symbols in Fig. 4 we reproduce the data for the device #3 from Supplementary Material Fig. S5F [15]. Solid lines are fits calculated using $\Delta S_V = 4k_B T_N (dv/di)$. Here, T_N is the noise temperature of the part of the device depicted in Fig. 1c and calculated using [25]

$$T_N = \frac{\int T(x,y)(\mathbf{j} \cdot \mathbf{E})\, dx\, dy}{\int (\mathbf{j} \cdot \mathbf{E})\, dx\, dy},$$

where $\mathbf{j}$ is the current density and $\mathbf{E}$ is the electric field in the given point of a device. Note that in the above expression for ΔS_V we neglect the nonequilibrium noise of device regions beyond those from Fig. 1c as well as the contribution from the amplifier noise due to the device resistance nonlinearity. Importantly, the fits go below the experimental data so that considering the amplifier

current noise and the contacts noise may become crucial in interpreting the data.

IV. Conclusion. In conclusion, we have discussed the recent strange metal experiment [15]. In the long device, resistivity, differential resistance and current noise data are self-consistent allowing us to extract low-temperature electron-phonon coupling, $\Sigma_{e-ph} = 9.6 \cdot 10^8\,\text{W/K}^{4.7}\text{m}^3$, and the temperature dependence of electron-phonon scattering length, $l_{e-ph} \propto T^{-1.7}$. In particular, at $T = 3\,\text{K}$ $l_{e-ph} \approx 1.4\,\mu\text{m}$ which is comparable to the constriction length in short devices. This finding demonstrates that electron-phonon scattering most likely can not be neglected in short devices making the statement on the failure of quasiparticle concept in YbRh$_2$Si$_2$ arguable. We have also considered the possible contribution of contact resistance and amplifiers noise to the experimental results. Overall, our findings provide information essential for further transport experiments.

We thank Liyang Chen and Douglas Natelson for valuable comments on the device fabrication details.

Conflict of interest. The authors of this work declare that they have no conflicts of interest.

---

1. H. V. Löhneysen, T. Pietrus, G. Portisch, H. G. Schlager, A. Schröder, M. Sieck, and T. Trappmann, Phys. Rev. Lett. **72**, 3262 (1994).

2. P. Fournier, P. Mohanty, E. Maiser, S. Darzens, T. Venkatesan, C. J. Lobb, G. Czjzek, R. A. Webb, and R. L. Greene, Phys. Rev. Lett. **81**, 4720 (1998).

3. A. Legros, S. Benhabib, W. Tabis, F. Laliberté, M. Dion, M. Lizaire, B. Vignolle, D. Vignolles, H. Raffy, Z. Z. Li, P. Auban-Senzier, N. Doiron-Leyraud, P. Fournier, D. Colson, L. Taillefer, and C. Proust, Nat. Phys. **15**, 142 (2019).

4. D. H. Nguyen, A. Sidorenko, M. Taupin, G. Knebel, G. Lapertot, E. Schuberth, and S. Paschen, Nat. Commun. **12**, 4341 (2021).

5. A. Jaoui, I. Das, G. Di Battista, J. Díez-Mérida, X. Lu, K. Watanabe, T. Taniguchi, H. Ishizuka, L. Levitov, and D. K. Efetov, Nat. Phys. **18**, 633 (2022).

6. V. R. Shaginyan, K. G. Popov, and V. A. Khodel, Phys. Rev. B **88**, 115103 (2013).

7. E. H. Hwang and S. Das Sarma, Phys. Rev. B **99**, 085105 (2019).

8. A. A. Patel and S. Sachdev, Phys. Rev. Lett. **123**, 066601 (2019).

9. V. R. Shaginyan, M. Ya. Amusia, A. Z. Msezane, V. A. Stephanovich, G. S. Japaridze, and S. A. Artamonov, JETP Lett. **110**, 290 (2019).

10. G. E. Volovik, JETP Lett. **110**, 352 (2019).

11. M. V. Sadovskii, JETP Lett. **111**, 188 (2020).

12. M. V. Sadovskii, Phys.-Uspekhi **64**, 175 (2021).

13. Y. Nakajima, T. Metz, C. Eckberg, K. Kirshenbaum, A. Hughes, R. Wang, L. Wang, S. R. Saha, I.-L. Liu, N. P. Butch, D. Campbell, Y. S. Eo, D. Graf, Z. Liu, S. V. Borisenko, P. Y. Zavalij, and J. Paglione, Commun. Phys. **3**, 181 (2020).

14. B. Michon, C. Berthod, C. W. Rischau, A. Ataei, L. Chen, S. Komiya, S. Ono, L. Taillefer, D. van Der Marel, and A. Georges, Nat. Commun. **14**, 3033 (2023).

15. L. Chen, D. T. Lowder, E. Bakali, A. M. Andrews, W. Schrenk, M. Waas, R. Svagera, G. Eguchi, L. Prochaska, Y. Wang, C. Setty, S. Sur, Q. Si, S. Paschen, and D. Natelson, Science **382**, 907 (2023).

16. V. R. Shaginyan, A. Z. Msezane, and G. S. Japaridze, arxiv:2312.16269 [cond-mat].

17. B. A. Polyak, E. S. Tikhonov, and V. S. Khrapai, arxiv:2401.08681 [cond-mat].

18. F. Giazotto, T. T. Heikkilä, A. Luukanen, A. M. Savin, and J. P. Pekola, Rev. Mod. Phys. **78**, 217 (2006).

19. A. O. Denisov, E. S. Tikhonov, S. U. Piatrusha, I. N. Khrapach, F. Rossella, M. Rocci, L. Sorba, S. Roddaro, and V. S. Khrapai, Nanotechnology **31**, 324004 (2020).

20. M. Reznikov, R. D. Picciotto, T. G. Griffiths, M. Heiblum, and V. Umansky, Nature **399**, 238 (1999).

21. E. S. Tikhonov, M. Yu. Melnikov, D. V. Shovkun, L. Sorba, G. Biasiol, and V. S. Khrapai, Phys. Rev. B **90**, 161405 (2014).

22. T. Muro, Y. Nishihara, S. Norimoto, M. Ferrier, T. Arakawa, K. Kobayashi, T. Ihn, C. Rössler, K. Ensslin, C. Reichl, and W. Wegscheider, Phys. Rev. B **93**, 195411 (2016).

23. T. Arakawa, Y. Nishihara, M. Maeda, S. Norimoto, and K. Kobayashi, Appl. Phys. Lett. **103**, 172104 (2013).

24. A. Nikolaenko, S. Sachdev, and A. A. Patel, Phys. Rev. Res. **5**, 043143 (2023).

25. S. U. Piatrusha, V. S. Khrapai, Z. D. Kvon, N. N. Mikhailov, S. A. Dvoretsky, and E. S. Tikhonov, Phys. Rev. B **96**, 245417 (2017).